Long-range *S*-wave *DD** interaction in covariant chiral effective field theory

Qing-Yu Zhai,[1] Ming-Zhu Liu,[2] Jun-Xu Lu,[1,*] and Li-Sheng Geng ®[1,3,4,5,†]

[1]*School of Physics, Beihang University, Beijing 102206, China*
[2]*School of Nuclear Science and Technology, Lanzhou University, Lanzhou 730000, China*
[3]*Peng Huanwu Collaborative Center for Research and Education, Beihang University,*
Beijing 100191, China
[4]*Beijing Key Laboratory of Advanced Nuclear Materials and Physics, Beihang University,*
Beijing 102206, China
[5]*Southern Center for Nuclear-Science Theory (SCNT), Institute of Modern Physics,*
Chinese Academy of Sciences, Huizhou 516000, Guangdong Province, China

Motivated by the recent lattice QCD study of the DD^* interaction at unphysical quark masses, we perform a theoretical study of the DD^* interaction in covariant chiral effective field theory. In particular, we calculate the relevant leading-order two-pion exchange contributions. The results compare favorably with the lattice QCD results, supporting the conclusion that the intermediate-range DD^* interaction is dominated by two-pion exchanges and the one-pion exchange contribution is absent. At a quantitative level, the covariant chiral perturbation theory results agree better with the lattice QCD results than their non-relativistic counterparts, showing the relevance of relativistic corrections in the charm sector.

I. INTRODUCTION

In 2021 the LHCb collaboration observed a narrow structure in the $D^0 D^0 \pi^+$ invariant mass spectrum of the pp interaction, identified as a doubly charmed tetraquark state, i.e., $T_{cc}^+(3875)$. It is natural to expect that the width of the T_{cc}^+ should be smaller than that of the D^{*+} [1–6]. Later, the LHCb collaboration analyzed their data with a resonance profile more suitable to account for the closeness of the T_{cc}^+ to the $D^{*+}D^0$ threshold, and the mass and width of T_{cc}^+ were found to be [7]

$$\delta m_{\text{pole}} = -360 \pm 40^{+4}_{-0} \text{ keV},$$
$$\Gamma_{\text{pole}} = 48 \pm 2^{+0}_{-14} \text{ keV}.$$

There were many theoretical studies predicting the existence of a $cc\bar{u}\bar{d}$ tetraquark before the experimental discovery [8–27]. The theoretical predictions for the mass of the $cc\bar{u}\bar{d}$ ground state with spin-parity quantum numbers $J^P = 1^+$ and isospin $I = 0$, relative to the $D^{*+}D^0$ mass threshold $\delta m = m_{T_{cc}^+} - (m_{D^0} + m_{D^{*+}})$, lies in the

range $-300 < \delta m < 300$ MeV. After the LHCb discovery, more studies were performed, and some of the earlier studies were updated. As the T_{cc}^+ state has a small binding energy and a narrow width, the molecular picture has gained a lot of attention [28–37]. In Ref. [1], the effective Lagrangian approach was used to investigate the decay width of T_{cc}^+, and the results support its molecular nature. In Ref. [35], the one-boson exchange potential model and the complex scaling method are used and T_{cc}^+ is shown to correspond to a quasibound state. In Ref. [37], the authors found that the possible contribution of a nonmolecular component or missing channels is smaller than 3%, which supported the molecular nature of T_{cc}^+. In addition, coupled-channel studies exist [2,3,30,32,38]. In Refs. [3,32], the authors studied the T_{cc}^+ in the $D^{*+}D^0$ and $D^{*0}D^+$ coupled channels and found a bound state corresponding to the T_{cc}^+, while in Ref. [38], $D^{*+}D^0$, $D^{*0}D^+$, and $D^{*0}D^{*+}$ coupled channels and the constituent quark model were used, and it was found that the $D^{*+}D^0$ component accounts for 86% of the T_{cc}^+ wave function. In addition to its production mechanisms and decay properties, its electromagnetic properties [39,40], the effects of three-body $DD\pi$ cut [32,41], the compositeness [42], and even the yield of T_{cc}^+ in heavy ion collisions [43] have been studied.

After the experimental discovery, several lattice QCD studies have been performed [44–46], In Ref. [44], a simulation of DD^* scattering for $m_\pi \simeq 280$ MeV was performed, and a doubly charmed tetraquark with $J^P = 1^+$ features as a virtual bound state in the simulation with a

*Corresponding author: ljxwohool@buaa.edu.cn
†Corresponding author: lisheng.geng@buaa.edu.cn

charm quark mass slightly larger than its physical value. In Ref. [45], the S-wave DD^* scattering in the isospin $I = 0, 1$ channels was studied for $m_\pi \simeq 350$ MeV. The authors found that the DD^* interaction in the $I = 0$ channel is attractive for a wide range of the DD^* energy, while the DD^* interaction induced by the charged ρ meson exchange may play a crucial role in the formation of $T_{cc}^+(3875)$.

It is particularly interesting to note that in Ref. [46], the DD^* interaction in the isoscalar and S-wave channel is studied for a nearly physical pion mass $m_\pi \simeq 146$ MeV, and the long-range part of the potential is found to be dominated by the two-pion exchange at least in the range $1 < r < 2$ fm.[1] In contrast, the one-pion exchange potential is absent. The overall attraction is strong enough to generate a near-threshold virtual state, which evolves into a loosely bound state for the physical $m_\pi \simeq 135$ MeV.

In Refs. [24,47], the one-pion and two-pion exchange potentials in the DD^* system were calculated in the nonrelativistic chiral effective field theory (ChEFT) up to the second and third order, respectively. It is interesting to note that in Ref. [47], the nonrelativistic ChEFT supports the dominance of the $ae^{-2m_\pi r}/r^2$ behavior of the two-pion exchange, similar to the lattice simulations but for ranges longer than $1 < r < 2$ fm. It was further pointed out that the $ae^{-2m_\pi r}/r^n$ behavior with $n > 2$ may also play a relevant role.

Motivated by the lattice QCD discovery of the dominant two-pion exchange potential [46] and the discrepancy between the nonrelativistic ChEFT and the lattice QCD simulations [47], we adopt the covariant ChEFT to calculate the two-pion-exchange contributions to the DD^* interaction, which are expected to converge faster. This is shown to be the case for baryon masses [48], magnetic moments [49,50], meson-baryon scattering [51–54], nucleon-nucleon scattering [55–59], hyperon-nucleon scattering [60–66], the $\Lambda_c N$ system [67,68], and the singly charmed meson sector [69–71]. However, covariant ChEFT has not been applied to study the systems of two charmed hadrons such as $DD^{(*)}(\bar{D}^{(*)})$ or $\Sigma_c^{(*)}\bar{D}^{(*)}$. The effective potential extracted by the HAL QCD method [72–76] provides a unique opportunity to investigate how covariance plays its role in such a heavy flavor system. That is, whether the covariant ChEFT can better describe the lattice QCD simulation [46].

This work is organized as follows. In Sec. II, we briefly explain the ChEFT approach and calculate the relevant Feynman diagrams. Results and discussions are given in Sec. III, followed by a summary in the last section. The analytical results for the pertinent Feynman diagrams are relegated to Appendices A and B. The heavy-meson

approximation and the comparison with the nonrelativistic results are in Appendix C.

II. THEORETICAL FORMALISM

A. Effective Lagrangians

In the framework of ChEFT, we can expand the amplitudes with a small parameter $\epsilon = \max\{p/\Lambda, m/\Lambda\}$, where p is the momentum of the pion, m is the pion mass or the $D - D^*$ mass splitting, and Λ is the breakdown scale of chiral symmetry or the mass of $D^{(*)}$ mesons.

In this work, we only consider the one-pion-exchange (OPE) diagram at the leading order (LO) $O(\epsilon^0)$ and the two-pion-exchange (TPE) diagram at the next-to-leading order (NLO) $O(\epsilon^2)$. For this, we first spell out the covariant chiral effective Lagrangian describing the interactions between charmed mesons D/D^* and Nambu-Goldstone bosons (NGB), which reads [77]

$$
\begin{aligned}
\mathcal{L} &= \langle \mathcal{D}_\mu P \mathcal{D}^\mu P \rangle - m_P^2 \langle P P^\dagger \rangle - \langle \mathcal{D}_\mu P^{*\nu} \mathcal{D}^\mu P_\nu^{*\dagger} \rangle \\
&+ m_{P^*}^2 \langle P^{*\nu} P_\nu^{*\dagger} \rangle + ig_D \langle P_\mu^* u^\mu P^\dagger - P u^\mu P_\mu^{*\dagger} \rangle \\
&+ \frac{g_{D^*}}{2} \langle (P_\mu^* u_\alpha \partial_\beta P_\nu^{*\dagger} - \partial_\beta P_\mu^* u_\alpha P_\nu^{*\dagger}) \epsilon^{\mu\nu\alpha\beta} \rangle,
\end{aligned}
\tag{1}
$$

where $P = (D^0, D^+, D_s^+)$ and $P^* = (D^{*0}, D^{*+}, D_s^{*+})_\mu$, the axial current is $u_\mu = i(\xi^\dagger \partial_\mu \xi - \xi \partial_\mu \xi^\dagger)$, and the chiral covariant derivative is

$$
\mathcal{D}_\mu P_a = \partial_\mu P_a - \Gamma_\mu^{ba} P_b, \qquad \mathcal{D}^\mu P_a^\dagger = \partial^\mu P_a^\dagger + \Gamma_{ab}^\mu P_b^\dagger, \tag{2}
$$

where $\Gamma_\mu = \frac{1}{2}(\xi^\dagger \partial_\mu \xi + \xi \partial_\mu \xi^\dagger)$ is the vector current. In the currents, $\xi^2 = \exp(i\Phi/f)$ with $f = 0.092$ GeV being the NGB decay constant in the chiral limit and Φ collecting the octet of NGB fields:

$$
\Phi = \sqrt{2}\begin{pmatrix} \frac{\pi^0}{\sqrt{2}} + \frac{\eta}{\sqrt{6}} & \pi^+ & K^+ \\ \pi^- & -\frac{\pi^0}{\sqrt{2}} + \frac{\eta}{\sqrt{6}} & K^0 \\ K^- & \bar{K}^0 & -\frac{2}{\sqrt{6}}\eta \end{pmatrix}. \tag{3}
$$

The coupling g_D is determined from the decay width of the D^{*+}, and the coupling g_{D^*} is related to g_D through the heavy-quark spin symmetry. The values of g_D and g_{D^*} are 1.177 GeV and $g_D/m_{D^*} = 0.583$, respectively [77,78].

B. Effective potentials of the DD^* system

At LO, the OPE diagram is illustrated in Fig. 1, which mainly contributes to the longest-range interaction. The OPE potential is

$$
V_{\text{OPE}} = A_{\text{OPE}}^I \cdot \frac{g_D^2}{f^2} \cdot \frac{(\epsilon_2 \cdot q)(\epsilon_4^\dagger \cdot q)}{q^2 - m_\pi^2 + i\epsilon}, \tag{4}
$$

---

[1]Note that in Ref. [47], $1 < r < 2$ fm is referred to as intermediate range. In this work, following Ref. [46], we refer to $1 < r < 2$ fm as long range.
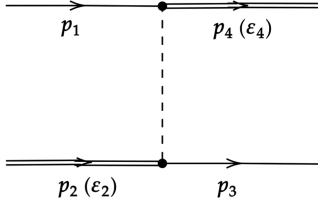
FIG. 1. One-pion exchange diagram at LO. The solid, double-solid, and dashed lines stand for D, D^*, and the pion, respectively.
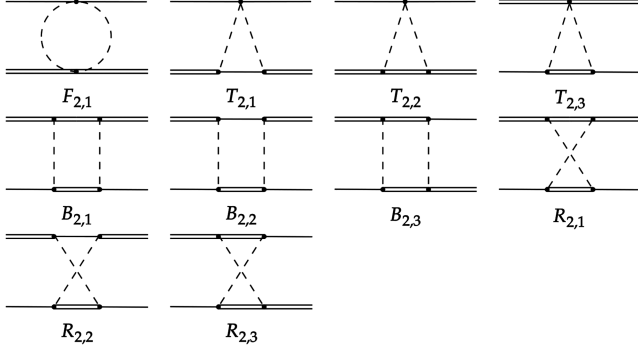

FIG. 2. Two-pion exchange diagrams at NLO. The solid, double-solid, and dashed lines represent D, D^* and the pion, respectively.

where $q = p_1 - p_4 = p_3 - p_2$, and ϵ_2 (ϵ_4) is the polarization vector of the D^* meson, and A^I_{OPE} is the isospin factor, where the superscript $I = 0, 1$ denotes the isospin of the DD^* system.

At NLO, there are ten TPE diagrams, which we illustrate in Fig. 2. One can calculate the TPE potential with the Lagrangian given in Eq. (1). Although the procedure is straightforward, the results are a bit tedious. Therefore, we relegate them to Appendix A. In Table I, we list the isospin factors appearing in Eqs. (4) and (A1)–(A10).

We calculate the effective potential in the center of mass system (c.m.s.) of the DD^* and project the potential to the S wave [79]

$$V(^{2S+1}L_J = {}^3S_1) = \frac{1}{2} \int d^3 p' V(\boldsymbol{p}, \boldsymbol{p}') \sin\theta \qquad (5)$$

TABLE I. Isospin factors for the OPE and TPE potentials of $DD^* \to DD^*$.

	A^I_{OPE}	$A^I_{F_{2,1}}$	$A^I_{T_{2,1}}$	$A^I_{T_{2,2}}$	$A^I_{T_{2,3}}$	$A^I_{B_{2,1}}$	$A^I_{B_{2,2}}$	$A^I_{B_{2,3}}$
$I = 0$	3	3	3	−3	−3	−9	9	9
$I = 1$	1	−1	−1	1	1	−1	1	−1

	$A^I_{R_{2,1}}$	$A^I_{R_{2,2}}$	$A^I_{R_{2,3}}$
$I = 0$	3	−3	−3
$I = 1$	−5	5	−5

where θ is the angle between $\boldsymbol{p}$ and $\boldsymbol{p}'$. We note that the Feynman diagrams $R_{2,1}$ and $R_{2,2}$ have a left-hand cut for $\theta \in [0, \pi]$, and therefore, we approximate $m_D = m_{D^*}$ in the dynamics but maintain the threshold of D and D^*, i.e., $m_D + m_{D^*}$, the same as the lattice simulations in the kinematics. According to the covariant power-counting rule based on naive dimensional analysis [77], $(m_{D^*} - m_D)$ is of order $\mathcal{O}(q^2)$. Thus, taking $(m_{D^*} - m_D)/\Lambda = 0$ in the TPE potential is a reasonable approximation, and the difference is of higher chiral order, which can be neglected.

We note that most TPE diagrams contain ultraviolet divergences, which the corresponding contact interactions of the same order should absorb. This, however, requires the introduction of unknown low-energy constants. In Ref. [24], these low-energy constants were determined in the resonance saturation approach. In the present work, as our main purpose is to check whether, for $1 \leq r \leq 2$ fm, the TPE contribution dominates the DD^* interaction, we take a different regularization approach, which is physically more intuitive. That is, we multiply each pion propagator with a monopole form factor[2]

$$F(q^2) = \frac{m_\pi^2 - \Lambda^2}{q^2 - \Lambda^2}, \qquad (6)$$

as is usually done in one-boson exchange models (see, e.g., Ref. [35]). We have checked that all the divergences originating from the dimensional regularization can be removed by $F(q^2)$, and the residual part can be considered the genuine two-pion exchange potential. Note that our covariant chiral TPE potential has dimension $[E]^0$, while the nonrelativistic ChEFT potential and the potential obtained in the lattice QCD simulation have dimension $[E]^{-2}$. Thus we divide our potential by $\sqrt{2m_D 2m_{D^*} 2m_D 2m_{D^*}}$ to set both dimensions the same, as is usually done in the nonrelativistic EFT [84,85].

C. Subtraction of the reducible part of the TPE potential

Note that the DD^* interaction extracted from lattice QCD simulations corresponds to the effective potential. As a result, we need to subtract from the amplitude of diagram $B_{2,2}$ the reducible part. Otherwise, double counting will occur when the effective potential is inserted into

---

[2]One should note that using form factors in chiral perturbation theory can potentially break chiral symmetry. In Refs. [80,81], it was shown that chiral symmetry is respected for loop functions containing only one pion propagator, as can be straightforwardly checked. On the other hand, this is not necessarily the case for the TPE diagrams studied in this work. Given its complexity, we will leave this issue for future work. We note that form factors are routinely used in dealing with nonperturbative strong interactions, such as the nucleon-nucleon interaction [82,83].
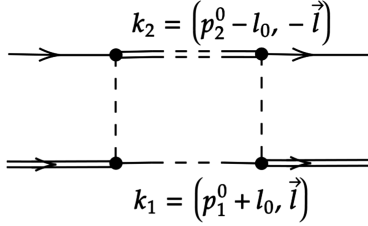
FIG. 3. The reducible part of the TPE potential from Feynmann diagram $B_{2,2}$, where $p_1^0 = s - m_{D^*}^2 + m_D^2/2\sqrt{s}$ and $p_2^0 = s + m_{D^*}^2 - m_D^2/2\sqrt{s}$.

the Kadyshevsky equation. The reducible part shown in Fig. 3 can be calculated in the following way:

$$V_{\mathrm{RP}} = i \int \frac{\mathrm{d}^4 l}{(2\pi)^4} \cdot \frac{V_{\mathrm{OPE}}(p,l)}{k_1^2 - m_1^2 + i\epsilon} \cdot \frac{V_{\mathrm{OPE}}(l,p')}{k_2^2 - m_2^2 + i\epsilon}, \quad (7)$$

$$\simeq \int \frac{\mathrm{d}l}{(2\pi)^3} \cdot \frac{l^2}{4E_1 E_2} \frac{V_{\mathrm{OPE}}(p,l) \cdot V_{\mathrm{OPE}}(l,p')}{\sqrt{s} - E_T + i\epsilon}, \quad (8)$$

where

$$k_1 = \left(\frac{s - m_{D^*}^2 + m_D^2}{2\sqrt{s}} + l_0, \boldsymbol{l} \right),$$

$$k_2 = \left(\frac{s + m_{D^*}^2 - m_D^2}{2\sqrt{s}} - l_0, -\boldsymbol{l} \right),$$

and $E_1 = \sqrt{l^2 + m_D^2}$, $E_2 = \sqrt{l^2 + m_{D^*}^2}$, $E_T = E_1 + E_2$.

To calculate the integral of Eq. (7), we put the momentum of D^* in V_{OPE} on shell and the momentum of D off shell, and close the l_0 contour integral in the lower half-plane with the pole located at $l_0^{(1)} = E_1 - (s - m_{D^*}^2 + m_D^2)/2\sqrt{s} - i\epsilon$ and $l_0^{(2)} = E_2 + (s + m_{D^*}^2 - m_D^2)/2\sqrt{s} - i\epsilon$. Then, Eq. (8) can be easily obtained using the residue theorem. The detailed calculation is given in Appendix A.

D. Lattice QCD DD^* potential in momentum space

The lattice QCD potential $V_{\mathrm{TPE}}^{\mathrm{L}}(r)$ is given in coordinate space [46],

$$V_{\mathrm{TPE}}^{\mathrm{L}}(r) = a_3 \frac{e^{-2m_\pi r}}{r^2}, \quad (9)$$

where $a_3 = -0.045$ GeV is the fitted parameter in the lattice simulation. To compare with the potential obtained in covariant ChEFT, we need to transform it into momentum space

$$V_{\mathrm{TPE}}^{\mathrm{L}}(\boldsymbol{q}) = \int \mathrm{d}^3 \boldsymbol{q} V_{\mathrm{TPE}}^{\mathrm{L}}(r) e^{-i\boldsymbol{q}\cdot\boldsymbol{r}}. \quad (10)$$

Performing the integration analytically, we obtain

$$V_{\mathrm{TPE}}^{\mathrm{L}}(q) = \tilde{a}_3 \frac{4\pi}{q} \arctan\left(\frac{q}{2m_\pi}\right), \quad (11)$$

where $\tilde{a}_3 \simeq -1.15$ GeV^{-1} is the fitted parameter in natural units, and $q = |\boldsymbol{q}| = \sqrt{p^2 + p'^2 - 2pp'\cos\theta}$, where $\boldsymbol{q}$ is the transfer momentum. Note that the potential of Eq. (11) should be projected to the S wave before it can be compared with both the relativistic and nonrelativistic chiral potentials.

It has been noticed that in Ref. [86], the potentials extracted by the HAL QCD method do not always match the intuitive expectation for baryon-baryon interactions. The potential from the HAL QCD method was much longer ranged and much stronger at larger distances than the intuitive expectations for the $\Omega\Omega$ [87] or ΩN [88] interaction where the pion exchanges cannot occur directly. On the other hand, for the interactions where the pion exchanges dominate the long-range part, such as the DD^* interaction studied here or the ΞN interaction [89], the HAL QCD method seems to be valid. Therefore, we treat the potential in Eq. (11) as a realistic interaction.

III. NUMERICAL RESULTS AND DISCUSSIONS

In this section, for the sake of convenience, we use $V_{\mathrm{OPE}}^{\mathrm{R}}$ and $V_{\mathrm{TPE}}^{\mathrm{R}}$ to denote our relativistic OPE and TPE potentials, respectively. $V_{\mathrm{TPE}}^{\mathrm{NR}}$ refers to the nonrelativistic TPE potential in momentum space derived in Ref. [47] and $V_{\mathrm{TPE}}^{\mathrm{L}}$ refers to the TPE potential given in Eq. (11) Fourier transformed from the lattice QCD potential [46].

We first compare our covariant chiral potentials with those obtained in the heavy meson chiral effective field theory (HMChEFT) [24]. The details of the analytic results are shown in the Appendix C, where at the nonrelativistic limit, i.e., $p \to 0$ and $m_{D^{(*)}} \to \infty$, our potentials have the same analytic structure as those of HMChEFT, as they should be. However, they will be different for finite momentum and heavy quark masses, as we will see later.

In Fig. 4, we show the contributions of various diagrams for a cutoff of $\Lambda \simeq 0.95$ GeV to match $V_{\mathrm{TPE}}^{\mathrm{L}}$ at $p = 0$. One can see that the relativistic TPE potential is dominated by diagram $B_{2,2}$ at $p \simeq 0$, or in the long range because the pion mass is close to the $D - D^*$ mass splitting. Thus, the four propagators of diagram $B_{2,2}$ can approach their on-shell conditions simultaneously and therefore enhance the contribution, which is the so-called box singularity [90]. The amplitude of diagram $B_{2,2}$ is also sensitive to the c.m.s. momentum and provides the dominant contribution to the momentum dependence of the TPE potential.

Next, in Fig. 5, we show the OPE and TPE potentials for a $\Lambda = 0.95$ GeV cutoff in the $I = 0$ channel. One can see that both the OPE and TPE potentials are attractive for all the ranges, and $V_{\mathrm{OPE}}^{\mathrm{R}} \simeq 0$ as $p \simeq 0$. In particular, V_{OPE} is much weaker than $V_{\mathrm{TPE}}^{\mathrm{R}}$ in the long range, which is
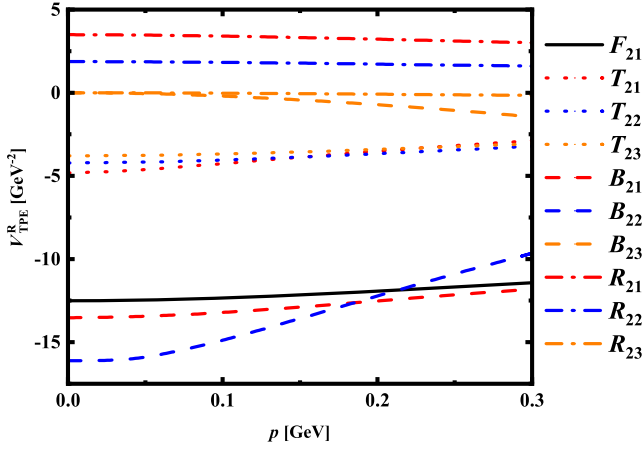
FIG. 4. Contributions of different Feynman diagrams as a function of $p = \sqrt{[s - (m_D + m_{D^*})^2][s - (m_D - m_{D^*})^2]}/2\sqrt{s}$ in the c.m.s. of DD^* for a cutoff of $\Lambda \simeq 0.95$ GeV.

consistent with the observation that V_{OPE} is absent in the lattice QCD simulation [46].

In Fig. 5, we also show the OPE and TPE potentials for the physical pion mass in the $I = 0$ channel. The interaction becomes more attractive than the potentials obtained with the lattice QCD pion mass. This is also consistent with the lattice QCD study where the potential for $m_\pi = 0.146$ GeV produces a virtual state, while a loosely bound state is generated for $m_\pi = 0.135$ GeV.

We also show the isovector OPE and TPE potentials in Fig. 5. They become comparable in the range of 0.05–0.3 GeV, and although both are attractive, they are
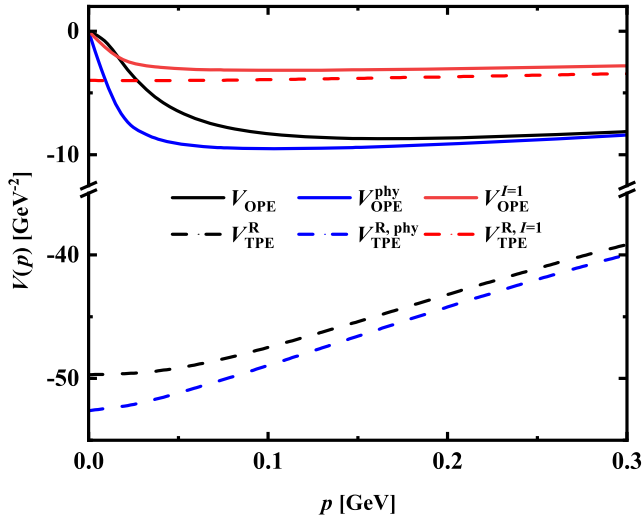
less attractive than their isoscalar counterparts. Since the isoscalar OPE and TPE potentials (black lines) can barely produce a virtual (or a loosely bound) state [46], and the contact interaction determined in the resonance saturation model is repulsive [24], we can assert that there exists no bound state in the $I = 1$ channel, consistent with Refs. [19,24,91].

In Fig. 6, we compare $V_{\text{TPE}}^{\text{L}}$, $V_{\text{TPE}}^{\text{R}}$, and $V_{\text{TPE}}^{\text{NR}}$. We set $\Lambda \simeq 0.95$ GeV for $V_{\text{TPE}}^{\text{R}}$ and $\Lambda \simeq 1.4$ GeV for $V_{\text{TPE}}^{\text{NR}}$ to match $V_{\text{TPE}}^{\text{L}}$ at $p = 0$. We can see that $V_{\text{TPE}}^{\text{R}}$ is consistent with $V_{\text{TPE}}^{\text{NR}}$ between 0 and 0.03 GeV, consistent with our analytic results shown in Appendix C. In addition, $V_{\text{TPE}}^{\text{R}}$ increases faster than $V_{\text{TPE}}^{\text{NR}}$ in the long-range (or in the small-momentum 0–0.3 GeV) region.

The different behavior between $V_{\text{TPE}}^{\text{NR}}$ and $V_{\text{TPE}}^{\text{R}}$ mainly originates from the nonrelativistic approximation, i.e., the neglect of terms of $\mathcal{O}(1/m_D)$ or higher order.

The lattice QCD simulations [46] show that in the range of $1 < r < 2$ fm, the DD^* interaction can be described by a TPE potential, i.e., Eq. (10) which corresponds to Eq. (11) in momentum space as shown in Fig. 6. In Ref. [47], it was revealed that $V_{\text{TPE}}^{\text{NR}}$ with a cutoff of $\Lambda \in [0.4, 0.9]$ GeV has the same asymptotic behavior as the lattice QCD potential, i.e., Eq. (10), but dominates the range longer than $1 < r < 2$ fm. This can be seen in Fig. 6—because $1 < r < 2$ fm corresponds to $0.07 < p < 0.15$ GeV approximately, a longer range corresponds to the momentum smaller than 0.07 GeV, while in Fig. 6 we can see that in the range of $0 < p < 0.03$ GeV especially, both $V_{\text{TPE}}^{\text{R}}$ and $V_{\text{TPE}}^{\text{NR}}$ are similar to $V_{\text{TPE}}^{\text{L}}$. In the range of $0 < p < 0.3$ GeV, with a reasonable cutoff, our covariant TPE potential can better describe $V_{\text{TPE}}^{\text{L}}$ than the nonrelativistic TPE.

FIG. 5. V_{OPE} and $V_{\text{TPE}}^{\text{R}}$ for different pion masses and different isospin channels for a cutoff $\Lambda \simeq 0.95$ GeV, where the solid lines denote the OPE potentials and the dashed lines denote the TPE potentials. The black and blue lines denote the potentials for $m_\pi = 0.146$ GeV, $m_D = 1.878$ GeV, $m_{D^*} = 2.018$ GeV, and $m_\pi = 0.138$ GeV, $m_D = 1.870$ GeV, $m_{D^*} = 2.007$ GeV. The red lines denote the OPE and TPE potentials in the $I = 1$ channel.
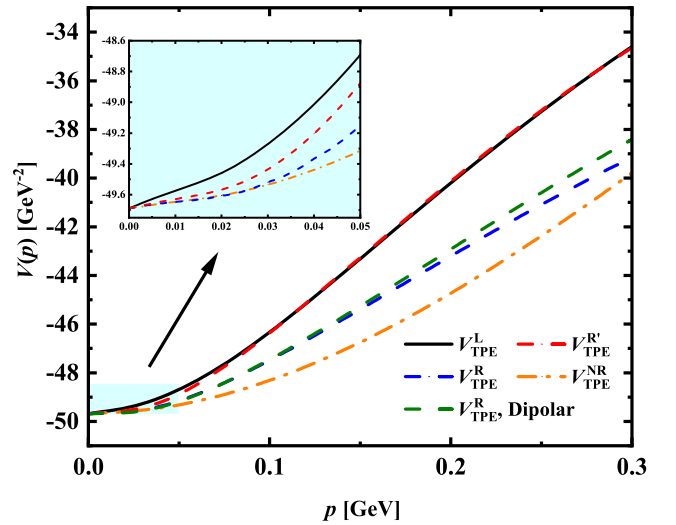

FIG. 6. $V_{\text{TPE}}^{\text{L}}$, $V_{\text{TPE}}^{\text{R}}$, and $V_{\text{TPE}}^{\text{NR}}$. We used a cutoff $\Lambda \simeq 0.95$ GeV for $V_{\text{TPE}}^{\text{R}}$ and $\Lambda \simeq 1.4$ GeV for $V_{\text{TPE}}^{\text{NR}}$ to match $V_{\text{TPE}}^{\text{L}}$ at $p = 0$. The $V_{\text{TPE}}^{\text{R}'}$ denoted by a red dashed line is the potential obtained with the unphysical parameter f with $\Lambda \simeq 0.74$ GeV.

Note that $V_{\text{TPE}}^{\text{R}}$ shown in Fig. 6 does not agree well with $V_{\text{TPE}}^{\text{L}}$. To understand whether this is due to the particular form factor we used, we tried a dipolar form factor instead of the monopolar one

$$F(q^2) = \left(\frac{m_\pi^2 - \Lambda^2}{q^2 - \Lambda^2}\right)^2$$

to consider the internal structure of the pion at each interaction vertex. The results are also shown in Fig. 6. We found that the dipolar form factor only improves the agreement between $V_{\text{TPE}}^{\text{R}}$ and $V_{\text{TPE}}^{\text{L}}$ a little bit, thus gives nearly the same description. Meanwhile, this nearly negligible improvement is at the expense of a large cutoff $\Lambda \simeq 1.6$ GeV, which is unreasonable in the chiral effective field theory. One notes that the potentials sensitively depend on the cutoff Λ in the monopole or dipole form factors. The form factors multiplied on the pion propagators allow the removal of spurious short-distance physics associated with high-momentum intermediate states. However, as mentioned previously, these cutoff momenta are determined by matching the lattice QCD results at the threshold, and we have not included any contact interactions. The cutoff here actually contains parts of the short-range contributions.

On the other hand, we believe that the differences between our $V_{\text{TPE}}^{\text{R}}$ and $V_{\text{TPE}}^{\text{L}}$ can be attributed to the fact that we used physical g_D and f and unphysical meson masses in the derivation of the TPE potential. The quark mass dependence of these quantities needs to be carefully taken into account for a proper comparison with the lattice QCD potential and is highly nontrivial. This goes beyond the scope of the present work. For demonstration, we replace f^{phy} with $f = C_\pi \cdot f^{\text{phy}}$. The results are shown in Fig. 6 for a cutoff $\Lambda \simeq 0.74$ GeV. With this reasonable cutoff, our TPE agrees well with $V_{\text{TPE}}^{\text{L}}$ in the range of $0.075 < p < 0.3$ GeV for $C_\pi \simeq 0.9$. Note that in Refs. [92,93], the m_π dependence of f_π up to NLO reads

$$f_\pi = f_\pi^{(0)}\left[1 - \frac{m_\pi^2}{4\pi^2(f_\pi^{(0)})^2}\log\left(\frac{m_\pi}{m_\pi^{\text{phy}}}\right) + \cdots\right],$$

which shows that a large m_π corresponds to a small f_π; thus, our use of a smaller f_π is reasonable. Overall, our results support the conclusion of the lattice QCD simulation that the TPE potential is dominant in the $1 < r < 2$ fm range.

IV. SUMMARY

In this work, we have studied the long-range S-wave DD^* interaction in covariant chiral effective field theory. In particular, we calculated the OPE and TPE potentials, regulated with a monopolar form factor $F(q^2)$. We found that Feynman diagram $B_{2,2}$ dominates the momentum dependence of the TPE potential. By comparing our OPE and TPE potentials, we found that, in the $I = 0$ channel, the TPE potential is dominant in the long range, and both potentials become more attractive as the pion mass approaches the physical point. While in the $I = 1$ channel, the OPE and TPE potentials are comparable and less attractive than those of the $I = 0$ channel. All the results are consistent with the lattice QCD study [46].

We compared our covariant TPE potential with the nonrelativistic one and the lattice QCD potential, and we found that all three potentials share nearly the same behavior in a range longer than 2 fm, while between 1 and 2 fm, our covariant TPE potential describes better the lattice QCD potential. We further demonstrated that with a smaller pion decay constant, e.g., by 10% compared with its physical value, one can better describe the lattice QCD potential with a reasonable cutoff. Overall, our study supports the conclusion of the lattice QCD study that the two-pion-exchange potential is dominant in the $1 < r < 2$ fm.

In Ref. [94], it was shown that the TPE potential also dominates the long-range $N\Phi$ potential. In Ref. [95], it was argued that the TPE potential can play a relevant role in the $J/\psi - J/\psi$ interaction. We plan to study these systems in chiral effective field theory.

APPENDIX A: COVARIANT TPE POTENTIAL

This Appendix shows the explicit expressions of the TPE potentials derived in covariant chiral effective field theory. They read as follows:

$$V_{F_{2,1}} = A_{F_{2,1}}^I \cdot \frac{1}{8f^4} \cdot \frac{1}{2} \int \frac{i\mathrm{d}^4l}{(2\pi)^4} \frac{[(p_2 + p_4)\cdot(p_2 - p_4 + 2l)][(p_1 + p_3)\cdot(p_2 - p_4 + 2l)]}{[(p_2 - p_4 + l)^2 - m^2 + i\epsilon](l^2 - m^2 + i\epsilon)}(\epsilon_2 \cdot \epsilon_4^\dagger), \qquad \text{(A1)}$$

$$V_{T_{2,1}} = A^I_{T_{2,1}} \cdot \frac{g_D^2}{2f^4} \int \frac{-i\mathrm{d}^4 l}{(2\pi)^4} \frac{[(p_4 - p_2 + l) \cdot \epsilon_4^\dagger][(p_1 + p_3) \cdot (p_4 - p_2 + 2l)](l \cdot \epsilon_2)}{[(p_2 - l)^2 - m_D^2 + i\epsilon](l^2 - m_\pi^2 + i\epsilon)[(p_4 - p_2 + l)^2 - m_\pi^2 + i\epsilon]} \tag{A2}$$

$$V_{T_{2,2}} = A^I_{T_{2,2}} \cdot \frac{g_{D^*}^2}{8f^4} \int \frac{-i\mathrm{d}^4 l}{(2\pi)^4} \epsilon^{\mu\nu\alpha\beta} \epsilon_4^{\dagger\nu}(p_4 - p_2 + l)^\alpha (p_2 + p_4 - l)^\beta \left[-g^{\mu\delta} + \frac{(p_2 - l)^\mu (p_2 - l)^\delta}{m_{D^*}^2} \right] \epsilon^{\lambda\delta\rho\sigma} \epsilon_2^\lambda l^\rho (2p_2 - l)^\sigma$$

$$\times \frac{(p_1 + p_3) \cdot (p_4 - p_2 + 2l)}{[(p_2 - l)^2 - m_{D^*}^2 + i\epsilon](l^2 - m_\pi^2 + i\epsilon)[(p_4 - p_2 + l)^2 - m_\pi^2 + i\epsilon]}, \tag{A3}$$

$$V_{T_{2,3}} = A^I_{T_{2,3}} \cdot \frac{g_D^2}{2f^4} \int \frac{-i\mathrm{d}^4 l}{(2\pi)^4} \frac{[(p_2 + p_4) \cdot (p_2 - p_4 + 2l)](\epsilon_2 \cdot \epsilon_4^\dagger)}{[(p_1 - l)^2 - m_D^2 + i\epsilon](l^2 - m_\pi^2 + i\epsilon)[(p_2 - p_4 + l)^2 - m_\pi^2 + i\epsilon]} (p_2 - p_4 + l)^\rho$$

$$\times \left[-g^{\rho\lambda} + \frac{(p_1 - l)^\rho (p_1 - l)^\lambda}{m_{D^*}^2} \right] l^\lambda, \tag{A4}$$

$$V_{B_{2,1}} = A^I_{B_{2,1}} \cdot \frac{g_D^2 g_{D^*}^2}{4f^4} \int \frac{i\mathrm{d}^4 l}{(2\pi)^4} \epsilon^{\mu\nu\alpha\beta} \epsilon_4^{\dagger\nu}(p_4 - p_2 + l)^\alpha (p_2 + p_4 - l)^\beta \left[-g^{\mu\lambda} + \frac{(p_2 - l)^\mu (p_2 - l)^\lambda}{m_{D^*}^2} \right] \epsilon^{\rho\lambda\sigma\eta} \epsilon_2^\rho l^\sigma (2p_2 - l)^\eta$$

$$\times \frac{(p_4 - p_2 + l)^\gamma [-g^{\gamma\delta} + \frac{(p_1 + l)^\gamma (p_1 + l)^\delta}{m_{D^*}^2}] l^\delta}{[(p_1 + l)^2 - m_{D^*}^2 + i\epsilon][(p_2 - l)^2 - m_{D^*}^2 + i\epsilon](l^2 - m_\pi^2 + i\epsilon)[(p_4 - p_2 + l)^2 - m_\pi^2 + i\epsilon]}, \tag{A5}$$

$$V_{B_{2,2}} = A^I_{B_{2,2}} \cdot \frac{g_D^4}{f^4} \int \frac{i\mathrm{d}^4 l}{(2\pi)^4} \frac{[(p_4 - p_2 + l) \cdot \epsilon_4^\dagger](\epsilon_2 \cdot l)}{[(p_1 + l)^2 - m_{D^*}^2 + i\epsilon][(p_2 - l)^2 - m_D^2 + i\epsilon](l^2 - m_\pi^2 + i\epsilon)[(p_4 - p_2 + l)^2 - m_\pi^2 + i\epsilon]}$$

$$\times l^\rho \left[-g^{\rho\lambda} + \frac{(p_1 + l)^\rho (p_1 + l)^\lambda}{m_{D^*}^2} \right] (p_4 - p_2 + l)^\lambda, \tag{A6}$$

$$V_{B_{2,3}} = A^I_{B_{2,3}} \cdot \frac{g_D^2 g_{D^*}^2}{4f^4} \int \frac{i\mathrm{d}^4 l}{(2\pi)^4} \epsilon^{\rho\sigma\delta\eta} \epsilon_2^\rho l^\sigma (2p_2 - l)^\eta \left[-g^{\delta\gamma} + \frac{(p_2 - l)^\delta (p_2 - l)^\gamma}{m_{D^*}^2} \right] (p_2 - p_3 - l)^\gamma$$

$$\times \frac{l^\lambda [-g^{\lambda\mu} + \frac{(p_1 + l)^\lambda (p_1 + l)^\mu}{m_{D^*}^2}] \epsilon^{\mu\nu\alpha\beta} \epsilon_4^{\dagger\nu}(p_2 - p_3 - l)^\alpha (p_1 + p_4 + l)^\beta}{[(p_1 + l)^2 - m_{D^*}^2 + i\epsilon][(p_2 - l)^2 - m_{D^*}^2 + i\epsilon](l^2 - m_\pi^2 + i\epsilon)[(p_2 - p_3 - l)^2 - m_\pi^2 + i\epsilon]}, \tag{A7}$$

$$V_{R_{2,1}} = A^I_{R_{2,1}} \cdot \frac{g_D^2 g_{D^*}^2}{4f^4} \int \frac{i\mathrm{d}^4 l}{(2\pi)^4} \epsilon^{\mu\nu\alpha\beta} \epsilon_4^{\dagger\nu}(p_4 - p_2 + l)^\alpha (p_2 + p_4 - l)^\beta \left[-g^{\mu\lambda} + \frac{(p_2 - l)^\mu (p_2 - l)^\lambda}{m_{D^*}^2} \right] \epsilon^{\rho\lambda\sigma\eta} \epsilon_2^\rho l^\sigma (2p_2 - l)^\eta$$

$$\times \frac{(p_4 - p_2 + l)^\gamma [-g^{\gamma\delta} + \frac{(p_3 - l)^\gamma (p_3 - l)^\delta}{m_{D^*}^2}] l^\delta}{[(p_3 - l)^2 - m_{D^*}^2 + i\epsilon][(p_2 - l)^2 - m_{D^*}^2 + i\epsilon](l^2 - m_\pi^2 + i\epsilon)[(p_4 - p_2 + l)^2 - m_\pi^2 + i\epsilon]}, \tag{A8}$$

$$V_{R_{2,2}} = A^I_{R_{2,2}} \cdot \frac{g_D^4}{f^4} \int \frac{i\mathrm{d}^4 l}{(2\pi)^4} \frac{[(p_4 - p_2 + l) \cdot \epsilon_4^\dagger](\epsilon_2 \cdot l)}{[(p_2 - l)^2 - m_D^2 + i\epsilon][(p_3 - l)^2 - m_{D^*}^2 + i\epsilon](l^2 - m_\pi^2 + i\epsilon)[(p_4 - p_2 + l)^2 - m_\pi^2 + i\epsilon]}$$

$$\times l^\rho \left[-g^{\rho\lambda} + \frac{(p_3 - l)^\rho (p_3 - l)^\lambda}{m_{D^*}^2} \right] (p_4 - p_2 + l)^\lambda, \tag{A9}$$

$$V_{R_{2,3}} = A^I_{R_{2,3}} \cdot \frac{g_D^2 g_{D^*}^2}{4f^4} \int \frac{i\mathrm{d}^4 l}{(2\pi)^4} \epsilon^{\rho\sigma\delta\eta} \epsilon_2^\rho l^\sigma (2p_2 - l)^\eta \left[-g^{\delta\gamma} + \frac{(p_2 - l)^\delta (p_2 - l)^\gamma}{m_{D^*}^2} \right] (p_3 - p_2 + l)^\gamma$$

$$\times \frac{(p_3 - p_2 + l)^\lambda [-g^{\lambda\mu} + \frac{(p_4 - l)^\lambda (p_4 - l)^\mu}{m_{D^*}^2}] \epsilon^{\mu\nu\alpha\beta} \epsilon_4^{\dagger\nu} l^\alpha (2p_4 - l)^\beta}{[(p_2 - l)^2 - m_{D^*}^2 + i\epsilon][(p_4 - l)^2 - m_{D^*}^2 + i\epsilon](l^2 - m_\pi^2 + i\epsilon)[(p_3 - p_2 + l)^2 - m_\pi^2 + i\epsilon]}. \tag{A10}$$

We calculate these loop integrals using dimensional regularization.

APPENDIX B: SUBTRACTION OF THE REDUCIBLE PART OF FEYNMAN DIAGRAM $B_{2,2}$

The reducible part of Feynman diagram $B_{2,2}$ is

$$V_{\text{RP}} = i \int \frac{\text{d}^4 l}{(2\pi)^4} \cdot \frac{V_{\text{OPE}}(p, l)}{k_1^2 - m_1^2 + i\epsilon} \cdot \frac{V_{\text{OPE}}(l, p')}{k_2^2 - m_2^2 + i\epsilon}, \quad \text{(B1)}$$

where

$$k_1 = \left(\frac{s - m_{D^*}^2 + m_D^2}{2\sqrt{s}} + l_0, \boldsymbol{l} \right),$$

$$k_2 = \left(\frac{s + m_{D^*}^2 - m_D^2}{2\sqrt{s}} - l_0, -\boldsymbol{l} \right).$$

To calculate Eq. (B1), we set D^* on shell, and D off shell, and obtain

$$V_{\text{RP}} \simeq i \int \frac{\text{d}^3 l}{(2\pi)^3} V_{\text{OPE}}(p, \sqrt{s} - E_2, E_2, \boldsymbol{l})$$

$$\times V_{\text{OPE}}(\sqrt{s} - E_2, E_2, \boldsymbol{l}, p')$$

$$\times \int \frac{dl_0}{2\pi} \cdot \frac{1}{k_1^2 - m_1^2 + i\epsilon} \cdot \frac{1}{k_2^2 - m_2^2 + i\epsilon}, \quad \text{(B2)}$$

where $E_2 = \sqrt{l^2 + m_{D^*}^2}$. The integral of l_0 can be calculated by using the residue theorem. We close the l_0 contour integral in the lower half-plane with the poles located at

$$l_0^{(1)} = E_1 - \frac{(s - m_{D^*}^2 + m_D^2)}{2\sqrt{s}} - i\epsilon,$$

$$l_0^{(2)} = E_2 + \frac{(s + m_{D^*}^2 - m_D^2)}{2\sqrt{s}} - i\epsilon,$$

where $E_1 = \sqrt{l^2 + m_D^2}$. Then we have

$$V_{\text{RP}} \simeq \int \frac{\text{d}^3 l}{(2\pi)^3} V_{\text{OPE}}(p, \sqrt{s} - E_2, E_2, \boldsymbol{l})$$

$$\times V_{\text{OPE}}(\sqrt{s} - E_2, E_2, \boldsymbol{l}, p') \cdot \frac{E_1 + E_2}{2 E_1 E_2} \cdot \frac{1}{s - E_T^2}, \quad \text{(B3)}$$

where $E_T = E_1 + E_2$. We use the approximation $\sqrt{s} \simeq E_T$, which is the same as reducing the Bethe-Salpeter equation to the Kadyshevsky equation. Then we have

$$V_{\text{RP}} = \int \frac{dl}{(2\pi)^3} \cdot \frac{l^2}{4 E_1 E_2} \frac{V_{\text{OPE}}(p, l) \cdot V_{\text{OPE}}(l, p')}{\sqrt{s} - E_T + i\epsilon},$$

$$= \mathcal{P} \int \frac{dl}{(2\pi)^3} \cdot \frac{l^2}{4 E_1 E_2} \frac{V_{\text{OPE}}(p, l) \cdot V_{\text{OPE}}(l, p')}{\sqrt{s} - E_T}$$

$$- i\pi \frac{1}{(2\pi)^3} \frac{p_{\text{cm}}}{4\sqrt{s}} V_{\text{OPE}}(p, p_{\text{cm}}) V_{\text{OPE}}(p_{\text{cm}}, p'), \quad \text{(B4)}$$

where $p_{\text{cm}} = \sqrt{[s - (m_D + m_{D^*})^2][s - (m_D - m_{D^*})^2]}/2\sqrt{s}$ is the momentum in the c.m.s., and $\mathcal{P}$ denotes the principal value of the integral.

In principle, the reducible parts of all the three box diagrams $B_{2,1}$, $B_{2,2}$, and $B_{2,3}$ should be subtracted. However, since we do not take into account the coupled channel of $DD^* \to D^* D^*$, and the energy region of our interest is below the threshold of $D^* D^*$, that is, the $D^* D^*$ channel does not open, there exists no double counting for the reducible parts of $B_{2,1}$ and $B_{2,3}$. Therefore only the reducible part of diagram $B_{2,2}$ is subtracted.

APPENDIX C: NONRELATIVISTIC APPROXIMATION OF THE COVARIANT NLO POTENTIAL

Following Refs. [24,96], one can decompose the potential to combinations of J functions employing the following tensor decomposition rules,

$$i \int \frac{\mu^{4-D} \text{d}^D l}{(2\pi)^D} \frac{\{1, l^\mu, l^\mu l^\rho, \cdots\}}{(l^2 - m_1^2 + i\epsilon)[(q + l)^2 - m_2^2 + i\epsilon]} \equiv \{\mathcal{J}_0^F, q^\mu \mathcal{J}_{11}^F, q^\mu q^\rho \mathcal{J}_{21}^F + g^{\mu\rho} J_{22}^F, \cdots\}, \quad \text{(C1)}$$

$$i \int \frac{\mu^{4-D} \text{d}^D l}{(2\pi)^D} \frac{\{1, l^\mu, l^\mu l^\nu, l^\mu l^\nu l^\rho, \cdots\}}{[(+/-)v \cdot l + \omega + i\epsilon](l^2 - m_1^2 + i\epsilon)[(q + l)^2 - m_2^2 + i\epsilon]}$$

$$\equiv \{\mathcal{J}_0^{T/S}, q^\mu \mathcal{J}_{11}^{T/S} + v^\mu \mathcal{J}_{12}^{T/S}, g^{\mu\nu} \mathcal{J}_{21}^{T/S} + q^\mu q^\nu \mathcal{J}_{22}^{T/S} + v^\mu v^\nu \mathcal{J}_{23}^{T/S} + (q \vee v) \mathcal{J}_{24}^{T/S},$$

$$(g \vee q) \mathcal{J}_{31}^{T/S} + q^\mu q^\nu q^\rho \mathcal{J}_{32}^{T/S} + (q^2 \vee v) \mathcal{J}_{33}^{T/S} + (g \vee v) \mathcal{J}_{34}^{T/S} + (q \vee v^2) \mathcal{J}_{35}^{T/S} + v^\mu v^\nu v^\rho \mathcal{J}_{36}^{T/S}, \cdots\}, \quad \text{(C2)}$$

$$i \int \frac{\mu^{4-D} \mathrm{d}^D l}{(2\pi)^D} \frac{\{1, l^\mu, l^\mu l^\nu, l^\mu l^\nu l^\rho, l^\mu l^\nu l^\rho l^\sigma, \cdots\}}{(v \cdot l + \omega_1 + i\epsilon)[(+/-)v \cdot l + \omega_2 + i\epsilon](l^2 - m_1^2 + i\epsilon)[(l+q)^2 - m_2^2 + i\epsilon]}$$

$$\equiv \{ \mathcal{J}_0^{R/B}, q^\mu \mathcal{J}_{11}^{R/B} + v^\mu \mathcal{J}_{12}^{R/B}, g^{\mu\nu} \mathcal{J}_{21}^{R/B} + q^\mu q^\nu \mathcal{J}_{22}^{R/B} + v^\mu v^\nu \mathcal{J}_{23}^{R/B} + (q \vee v) \mathcal{J}_{24}^{R/B},$$

$$(g \vee q) \mathcal{J}_{31}^{R/B} + q^\mu q^\nu q^\rho \mathcal{J}_{32}^{R/B} + (q^2 \vee v) \mathcal{J}_{33}^{R/B} + (g \vee v) \mathcal{J}_{34}^{R/B} + (q \vee v^2) \mathcal{J}_{35}^{R/B} + v^\mu v^\nu v^\rho \mathcal{J}_{36}^{R/B},$$

$$(g \vee g) \mathcal{J}_{41}^{R/B} + (g \vee q^2) \mathcal{J}_{42}^{R/B} + q^\mu q^\nu q^\rho q^\sigma \mathcal{J}_{43}^{R/B} + (g \vee v^2) \mathcal{J}_{44}^{R/B} + v^\mu v^\nu v^\rho v^\sigma \mathcal{J}_{45}^{R/B} + (q^3 \vee v) \mathcal{J}_{46}^{R/B}$$

$$+ (q^2 \vee v^2) \mathcal{J}_{47}^{R/B} + (q \vee v^3) \mathcal{J}_{48}^{R/B} + (g \vee q \vee v) \mathcal{J}_{49}^{R/B}, \cdots \}. \tag{C3}$$

More specifically, we follow the following steps to perform the nonrelativistic reduction of our covariant potentials:

(1) Rewrite the denominator

Note that the expression of the J functions can be derived by the heavy meson approach, that is

$$p_\mu = m v_\mu + k_\mu \quad \text{with} \quad v^2 = 1, \tag{C4}$$

where k^2 is infinitesimal and can be neglected.

(2) Rewrite the momentum.

We approximate the momentum with the velocity, i.e.,

$$\frac{p_\mu}{m} \simeq v_\mu \tag{C5}$$

and set $m_D = m_{D^*} = m$. In Refs. [24,96], the definition of q and p is $q = p_1 - p_3$ and $p = p_1 - p_4$, we take the following limits

$$p_2 \cdot \epsilon_2 \to 0, \quad p_4 \cdot \epsilon_4 \to 0,$$

$$p_2 \cdot \epsilon_4 \to -q \cdot \epsilon_4, \quad p_1 \cdot \epsilon_4 \to p \cdot \epsilon_4,$$

$$p_3 \cdot \epsilon_2 \to p \cdot \epsilon_2, \quad p_4 \cdot \epsilon_2 \to q \cdot \epsilon_2,$$

$$p_1 \cdot \epsilon_2 \to q \cdot \epsilon_2 + p \cdot \epsilon_2, \quad p_3 \cdot \epsilon_4 \to p \cdot \epsilon_4 - q \cdot \epsilon_4. \tag{C6}$$

In such limits, $\boldsymbol{p}_1 = -\boldsymbol{p}_2 = (0, 0, \tilde{p})$, $\boldsymbol{p}_3 = -\boldsymbol{p}_4 = (\tilde{p} \sin\theta, 0, \tilde{p} \cos\theta)$. Thus $\boldsymbol{q}^2 = (\boldsymbol{p}_1 - \boldsymbol{p}_3)^2 = 2\tilde{p}^2(1 - \cos\theta)$, $\boldsymbol{p}^2 = (\boldsymbol{p}_1 - \boldsymbol{p}_4)^2 = 2\tilde{p}^2(1 + \cos\theta)$.

(3) Calculate the coefficient of the integrated tensor, and do the nonrelativistic approximation.

We explain this procedure using $V_{F_{2,1}}$ as an example. In obtaining $V_{F_{2,1}}$, we need to calculate the following integral

$$i \int \frac{\mu^{4-D} \mathrm{d}^D l}{(2\pi)^D} \frac{\{1, l^\mu, l^\mu l^\nu\}}{(l^2 - m^2 + i\epsilon)[(l-q)^2 - m^2 + i\epsilon]},$$

which equals to $\mathcal{J}_0^F$, $-q^\mu \mathcal{J}_{11}^F$, and $q^\mu q^\rho \mathcal{J}_{21}^F + g^{\mu\rho} J_{22}^F$ in the nonrelativistic ChEFT, respectively. One can see that the coefficients of these three tensors are

$$0, 0, 4i(\epsilon_2 \cdot \epsilon_4^*)(p_1 + p_3)^\mu (p_2 + p_4)^\nu.$$

After the contraction and under the nonrelativistic approximation, we have

$$V_{F_{2,1}}^{\mathrm{R}} = \frac{1}{2} \cdot \frac{3}{8f^4} \cdot 16 m_D m_{D^*} (\epsilon_2 \cdot \epsilon_4^*) \mathcal{J}_{22}^F$$

$$= V_{F_{2,1}}^{\mathrm{NR}} \cdot 4 m_D m_{D^*}. \tag{C7}$$

We also elaborate on $V_{T_{2,1}}^{\mathrm{R}}$ as an example. Our covariant potential has the following structure

$$i \int \frac{\mathrm{d}^4 l}{(2\pi)^4} \frac{\{1, l^\mu, l^\mu l^\nu, l^\mu l^\nu l^\rho, \cdots\}}{[(p_2 - l)^2 - m_D^2 + i\epsilon](l^2 - m_\pi^2 + i\epsilon)[(q+l)^2 - m_\pi^2 + i\epsilon]}. \tag{C8}$$

According to the heavy meson approach, we deal with the first denominator by replacing $(p_2 - l)_\mu = m_D v_\mu + k_\mu$, and therefore have

$$(p_2 - l)^2 - m_D^2 \simeq 2 m_D v \cdot k = 2 m_D(-v \cdot l + v \cdot p_2 - m_D). \tag{C9}$$

We rewrite $\omega = v \cdot p_2 - m_D \simeq \Delta$, and under the nonrelativistic approximation, we have

$$i \int \frac{\mathrm{d}^4 l}{(2\pi)^4} \frac{\{1, l^\mu, l^\mu l^\nu, l^\mu l^\nu l^\rho, \cdots\}}{[(p_2 - l)^2 - m_D^2 + i\epsilon](l^2 - m_\pi^2 + i\epsilon)[(q + l)^2 - m_\pi^2 + i\epsilon]}$$

$$\simeq \frac{i}{2m_D} \int \frac{\mathrm{d}^4 l}{(2\pi)^4} \frac{\{1, l^\mu, l^\mu l^\nu, l^\mu l^\nu l^\rho, \cdots\}}{(-v \cdot l + \omega + i\epsilon)(l^2 - m_\pi^2 + i\epsilon)[(l + q)^2 - m_\pi^2 + i\epsilon]},$$

$$\equiv \frac{1}{2m_D} \{ \mathcal{J}_0^S, q^\mu \mathcal{J}_{11}^S + v^\mu \mathcal{J}_{12}^S, g^{\mu\nu} \mathcal{J}_{21}^S + q^\mu q^\nu \mathcal{J}_{22}^S + v^\mu v^\nu \mathcal{J}_{23}^S + (q \vee v) \mathcal{J}_{24}^S,$$

$$(g \vee q) \mathcal{J}_{31}^S + q^\mu q^\nu q^\rho \mathcal{J}_{32}^S + (q^2 \vee v) \mathcal{J}_{33}^S + (g \vee v) \mathcal{J}_{34}^S + (q \vee v^2) \mathcal{J}_{35}^S + v^\mu v^\nu v^\rho \mathcal{J}_{36}^S, \cdots\},$$

$$\simeq \frac{1}{2m_D} \left\{ \mathcal{J}_0^S, q^\mu \mathcal{J}_{11}^S + \frac{p_2^\mu}{m_{D^*}} \mathcal{J}_{12}^S, g^{\mu\nu} \mathcal{J}_{21}^S + q^\mu q^\nu \mathcal{J}_{22}^S + \frac{p_2^\mu p_2^\nu}{m_{D^*}^2} \mathcal{J}_{23}^S + \frac{q \vee p_2}{m_{D^*}} \mathcal{J}_{24}^S, \right.$$

$$\left. (g \vee q) \mathcal{J}_{31}^S + q^\mu q^\nu q^\rho \mathcal{J}_{32}^S + \frac{q^2 \vee p_2}{m_{D^*}} \mathcal{J}_{33}^S + \frac{g \vee p_2}{m_{D^*}} \mathcal{J}_{34}^S + \frac{q \vee p_2^2}{m_{D^*}^2} \mathcal{J}_{35}^S + \frac{p_2^\mu p_2^\nu p_2^\rho}{m_{D^*}^3} \mathcal{J}_{36}^S, \cdots \right\}. \tag{C10}$$

Contract with the coefficients and do the nonrelativistic approximation, we finally obtain

$$V_{T_{2,1}}^{\mathrm{NR}} = \frac{3g^2}{f^4} [(\epsilon_2 \cdot \epsilon_4^*) \cdot \mathcal{J}_{34}^S + (q \cdot \epsilon_2)(q \cdot \epsilon_4^*)(\mathcal{J}_{24}^S + \mathcal{J}_{33}^S)](m_\pi, \Delta, |\boldsymbol{q}|) \cdot \left(-\frac{1}{4}\right), \tag{C11}$$

$$V_{T_{2,1}}^{\mathrm{R}} = \frac{3g_D^2}{2f^4} [-4m_D m_{D^*}(q \cdot \epsilon_2)(q \cdot \epsilon_4^*) \cdot \mathcal{J}_{24}^S - 4m_D m_{D^*}(q \cdot \epsilon_2)(q \cdot \epsilon_4^*) \cdot \mathcal{J}_{33}^S - 4m_D m_{D^*}(\epsilon_2 \cdot \epsilon_4^*) \cdot \mathcal{J}_{34}^S] \frac{1}{2m_D m_{D^*}},$$

$$= V_{T_{2,1}}^{\mathrm{NR}} \cdot \frac{g_D^2}{g^2} \cdot 4. \tag{C12}$$

Note that in our covariant potential, the order of the integrated tensor may be higher than what we have shown in Eqs. (C1)–(C3). However, since $l^\mu l^\nu / m_{D^{(*)}}^2 \simeq 0$, the problem does not matter.

From the steps shown above, after dividing our potentials by $\sqrt{2m_D 2m_{D^*} 2m_D 2m_{D^*}}$ according to Refs. [84,85], and note that $g_{D^*} \simeq g$, it is obvious that after taking the nonrelativistic approximation, our covariant TPE potential is the same as the HMChEFT one.

[1] X.-Z. Ling, M.-Z. Liu, L.-S. Geng, E. Wang, and J.-J. Xie, Phys. Lett. B **826**, 136897 (2022).

[2] L. Meng, G.-J. Wang, B. Wang, and S.-L. Zhu, Phys. Rev. D **104**, L051502 (2021).

[3] A. Feijoo, W. H. Liang, and E. Oset, Phys. Rev. D **104**, 114015 (2021).

[4] M.-J. Yan and M. P. Valderrama, Phys. Rev. D **105**, 014007 (2022).

[5] S. Fleming, R. Hodges, and T. Mehen, Phys. Rev. D **104**, 116010 (2021).

[6] L. Dai, S. Fleming, R. Hodges, and T. Mehen, Phys. Rev. D **107**, 076001 (2023).

[7] R. Aaij et al. (LHCb Collaboration), Nat. Commun. **13**, 3351 (2022).

[8] J. Carlson, L. Heller, and J. A. Tjon, Phys. Rev. D **37**, 744 (1988).

[9] B. Silvestre-Brac and C. Semay, Z. Phys. C **57**, 273 (1993).

[10] C. Semay and B. Silvestre-Brac, Z. Phys. C **61**, 271 (1994).

[11] M. A. Moinester, Z. Phys. A **355**, 349 (1996).

[12] S. Pepin, F. Stancu, M. Genovese, and J. M. Richard, Phys. Lett. B **393**, 119 (1997).

[13] B. A. Gelman and S. Nussinov, Phys. Lett. B **551**, 296 (2003).

[14] J. Vijande, F. Fernandez, A. Valcarce, and B. Silvestre-Brac, Eur. Phys. J. A **19**, 383 (2004).

[15] D. Janc and M. Rosina, Few-Body Syst. **35**, 175 (2004).

[16] J. Vijande, E. Weissman, A. Valcarce, and N. Barnea, Phys. Rev. D **76**, 094027 (2007).

[17] S. H. Lee and S. Yasui, Eur. Phys. J. C **64**, 283 (2009).

[18] Y. Yang, C. Deng, J. Ping, and T. Goldman, Phys. Rev. D **80**, 114023 (2009).

[19] N. Li, Z.-F. Sun, X. Liu, and S.-L. Zhu, Phys. Rev. D **88**, 114008 (2013).

[20] G. Q. Feng, X. H. Guo, and B. S. Zou, arXiv:1309.7813.

[21] M. Karliner and J. L. Rosner, Phys. Rev. Lett. **119**, 202001 (2017).

[22] S.-Q. Luo, K. Chen, X. Liu, Y.-R. Liu, and S.-L. Zhu, Eur. Phys. J. C **77**, 709 (2017).

[23] Z.-G. Wang, Acta Phys. Pol. B **49**, 1781 (2018).

[24] H. Xu, B. Wang, Z.-W. Liu, and X. Liu, Phys. Rev. D **99,** 014027 (2019); **104,** 119903(E) (2021).

[25] P. Junnarkar, N. Mathur, and M. Padmanath, Phys. Rev. D **99,** 034507 (2019).

[26] M.-Z. Liu, T.-W. Wu, M. Pavon Valderrama, J.-J. Xie, and L.-S. Geng, Phys. Rev. D **99,** 094018 (2019).

[27] Q. Qin, Y.-F. Shen, and F.-S. Yu, Chin. Phys. C **45,** 103106 (2021).

[28] K. Chen, R. Chen, L. Meng, B. Wang, and S.-L. Zhu, Eur. Phys. J. C **82,** 581 (2022).

[29] H. Ren, F. Wu, and R. Zhu, Adv. High Energy Phys. **2022,** 9103031 (2022).

[30] M. Albaladejo, Phys. Lett. B **829,** 137052 (2022).

[31] X.-K. Dong, F.-K. Guo, and B.-S. Zou, Commun. Theor. Phys. **73,** 125201 (2021).

[32] M.-L. Du, V. Baru, X.-K. Dong, A. Filin, F.-K. Guo, C. Hanhart, A. Nefediev, J. Nieves, and Q. Wang, Phys. Rev. D **105,** 014024 (2022).

[33] Q. Xin and Z.-G. Wang, Eur. Phys. J. A **58,** 110 (2022).

[34] H.-W. Ke, X.-H. Liu, and X.-Q. Li, Eur. Phys. J. C **82,** 144 (2022).

[35] J.-B. Cheng, Z.-Y. Lin, and S.-L. Zhu, Phys. Rev. D **106,** 016012 (2022).

[36] S. S. Agaev, K. Azizi, and H. Sundu, J. High Energy Phys. 06 (2022) 057.

[37] L. R. Dai, L. M. Abreu, A. Feijoo, and E. Oset, Eur. Phys. J. C **83,** 983 (2023).

[38] P. G. Ortega, J. Segovia, D. R. Entem, and F. Fernandez, Phys. Lett. B **841,** 137918 (2023).

[39] C. Deng and S.-L. Zhu, Phys. Rev. D **105,** 054015 (2022).

[40] U. Özdem, Phys. Rev. D **105,** 054019 (2022).

[41] M.-L. Du, A. Filin, V. Baru, X.-K. Dong, E. Epelbaum, F.-K. Guo, C. Hanhart, A. Nefediev, J. Nieves, and Q. Wang, Phys. Rev. Lett. **131,** 131903 (2023).

[42] T. Kinugawa and T. Hyodo, arXiv:2303.07038.

[43] Y. Hu, J. Liao, E. Wang, Q. Wang, H. Xing, and H. Zhang, Phys. Rev. D **104,** L111502 (2021).

[44] M. Padmanath and S. Prelovsek, Phys. Rev. Lett. **129,** 032002 (2022).

[45] S. Chen, C. Shi, Y. Chen, M. Gong, Z. Liu, W. Sun, and R. Zhang, Phys. Lett. B **833,** 137391 (2022).

[46] Y. Lyu, S. Aoki, T. Doi, T. Hatsuda, Y. Ikeda, and J. Meng, Phys. Rev. Lett. **131,** 161901 (2023).

[47] B. Wang and L. Meng, Phys. Rev. D **107,** 094002 (2023).

[48] X. L. Ren, L. S. Geng, J. Martin Camalich, J. Meng, and H. Toki, J. High Energy Phys. 12 (2012) 073.

[49] L. S. Geng, J. Martin Camalich, L. Alvarez-Ruso, and M. J. Vicente Vacas, Phys. Rev. Lett. **101,** 222002 (2008).

[50] Y. Xiao, X.-L. Ren, J.-X. Lu, L.-S. Geng, and U.-G. Meißner, Eur. Phys. J. C **78,** 489 (2018).

[51] J. M. Alarcon, J. Martin Camalich, and J. A. Oller, Phys. Rev. D **85,** 051503 (2012).

[52] Y.-H. Chen, D.-L. Yao, and H. Q. Zheng, Phys. Rev. D **87,** 054019 (2013).

[53] J.-X. Lu, L.-S. Geng, X.-L. Ren, and M.-L. Du, Phys. Rev. D **99,** 054024 (2019).

[54] J.-X. Lu, L.-S. Geng, M. Doering, and M. Mai, Phys. Rev. Lett. **130,** 071902 (2023).

[55] X.-L. Ren, K.-W. Li, L.-S. Geng, B.-W. Long, P. Ring, and J. Meng, Chin. Phys. C **42,** 014103 (2018).

[56] Y. Xiao, L.-S. Geng, and X.-L. Ren, Phys. Rev. C **99,** 024004 (2019).

[57] X.-L. Ren, C.-X. Wang, K.-W. Li, L.-S. Geng, and J. Meng, Chin. Phys. Lett. **38,** 062101 (2021).

[58] C.-X. Wang, L.-S. Geng, and B. Long, Chin. Phys. C **45,** 054101 (2021).

[59] J.-X. Lu, C.-X. Wang, Y. Xiao, L.-S. Geng, J. Meng, and P. Ring, Phys. Rev. Lett. **128,** 142002 (2022).

[60] K.-W. Li, X.-L. Ren, L.-S. Geng, and B. Long, Phys. Rev. D **94,** 014029 (2016).

[61] K.-W. Li, X.-L. Ren, L.-S. Geng, and B.-W. Long, Chin. Phys. C **42,** 014105 (2018).

[62] K.-W. Li, T. Hyodo, and L.-S. Geng, Phys. Rev. C **98,** 065203 (2018).

[63] J. Song, K.-W. Li, and L.-S. Geng, Phys. Rev. C **97,** 065201 (2018).

[64] Z.-W. Liu, J. Song, K.-W. Li, and L.-S. Geng, Phys. Rev. C **103,** 025201 (2021).

[65] J. Song, Z.-W. Liu, K.-W. Li, and L.-S. Geng, Phys. Rev. C **105,** 035203 (2022).

[66] Z.-W. Liu, K.-W. Li, and L.-S. Geng, Chin. Phys. C **47,** 024108 (2023).

[67] J. Song, Y. Xiao, Z.-W. Liu, C.-X. Wang, K.-W. Li, and L.-S. Geng, Phys. Rev. C **102,** 065208 (2020).

[68] J. Song, Y. Xiao, Z.-W. Liu, K.-W. Li, and L.-S. Geng, Commun. Theor. Phys. **75,** 015202 (2023).

[69] D.-L. Yao, M.-L. Du, F.-K. Guo, and U.-G. Meißner, J. High Energy Phys. 11 (2015) 058.

[70] M.-L. Du, F.-K. Guo, U.-G. Meißner, and D.-L. Yao, Phys. Rev. D **94,** 094037 (2016).

[71] M.-L. Du, F.-K. Guo, U.-G. Meißner, and D.-L. Yao, Eur. Phys. J. C **77,** 728 (2017).

[72] N. Ishii, S. Aoki, and T. Hatsuda, Phys. Rev. Lett. **99,** 022001 (2007).

[73] N. Ishii, S. Aoki, T. Doi, T. Hatsuda, Y. Ikeda, T. Inoue, K. Murano, H. Nemura, and K. Sasaki (HAL QCD Collaboration), Phys. Lett. B **712,** 437 (2012).

[74] S. Aoki and T. Doi, Front. Phys. **8,** 307 (2020).

[75] S. Aoki, N. Ishii, T. Doi, T. Hatsuda, Y. Ikeda, T. Inoue, K. Murano, H. Nemura, and K. Sasaki (HAL QCD Collaboration), Proc. Jpn. Acad. Ser. B **87,** 509 (2011).

[76] T. Iritani, S. Aoki, T. Doi, T. Hatsuda, Y. Ikeda, T. Inoue, N. Ishii, H. Nemura, and K. Sasaki (HAL QCD Collaboration), J. High Energy Phys. 03 (2019) 007.

[77] M. Altenbuchinger, L. S. Geng, and W. Weise, Phys. Rev. D **89,** 014026 (2014).

[78] X.-Z. Ling, J.-X. Lu, M.-Z. Liu, and L.-S. Geng, Phys. Rev. D **104,** 074022 (2021).

[79] J. Golak *et al.*, Eur. Phys. J. A **43,** 241 (2010).

[80] J. F. Donoghue, B. R. Holstein, and B. Borasoy, Phys. Rev. D **59,** 036002 (1999).

[81] J. F. Donoghue and B. R. Holstein, Phys. Lett. B **436,** 331 (1998).

[82] R. Machleidt and D. R. Entem, Phys. Rep. **503,** 1 (2011).

[83] P. Reinert, H. Krebs, and E. Epelbaum, Eur. Phys. J. A **54,** 86 (2018).

[84] V. Antonelli, A. Gall, J. Gasser, and A. Rusetsky, Ann. Phys. (N.Y.) **286,** 108 (2001).

[85] U.-G. Meißner and A. Rusetsky, *Effective Field Theories* (Cambridge University Press, Cambridge, England, 2022), 10.1017/9781108689038.

[86] J. Haidenbauer and U.-G. Meißner, Eur. Phys. J. A **55**, 70 (2019).

[87] S. Gongyo *et al.*, Phys. Rev. Lett. **120**, 212001 (2018).

[88] T. Iritani *et al.* (HAL QCD Collaboration), Phys. Lett. B **792**, 284 (2019).

[89] K. Sasaki, S. Aoki, T. Doi, S. Gongyo, T. Hatsuda, Y. Ikeda, T. Inoue, T. Iritani, N. Ishii, and T. Miyamoto (HAL QCD Collaboration), EPJ Web Conf. **175**, 05010 (2018).

[90] M.-X. Duan, L. Qiu, X.-Z. Ling, and Q. Zhao, arXiv:2303.13329.

[91] S. Ohkoda, Y. Yamaguchi, S. Yasui, K. Sudoh, and A. Hosaka, Phys. Rev. D **86**, 034019 (2012).

[92] J. Gasser and H. Leutwyler, Ann. Phys. (N.Y.) **158**, 142 (1984).

[93] S. R. Beane and M. J. Savage, Nucl. Phys. **A717**, 91 (2003).

[94] Y. Lyu, T. Doi, T. Hatsuda, Y. Ikeda, J. Meng, K. Sasaki, and T. Sugiura, Phys. Rev. D **106**, 074507 (2022).

[95] X.-K. Dong, V. Baru, F.-K. Guo, C. Hanhart, A. Nefediev, and B.-S. Zou, Sci. Bull. **66**, 2462 (2021).

[96] B. Wang, Z.-W. Liu, and X. Liu, Phys. Rev. D **99**, 036007 (2019).